CHINESE OPTICS LETTERS

Vol. 20, No. 1 | January 2022

Bioinspired lenses from cats' eyes

Shuwen Xue (薛淑雯), Chuanjie Hu (胡传捷), Miao Zhang (张 淼), and Huanyang Chen (陈焕阳)*

Institute of Electromagnetics and Acoustics and Department of Physics, Xiamen University, Xiamen 361005, China

*Corresponding author: kenyon@xmu.edu.cn

Received July 6, 2021 | Accepted July 30, 2021 | Posted Online September 28, 2021

It is well known that cats have fascinating eyes with various colors, such as green, blue, and brown. In addition, they possess strong night vision ability, which can distinguish things clearly even in a poor light environment. These drive us to reveal the secrets behind them. In fact, cats' eyes can be considered as special lenses (which we would like to mimic by using a Luneburg lens). We make an analysis of the role of photonic crystals behind the lens and demonstrate that the integration of photonic crystals into Luneburg lens can be regarded as a retroreflector and greatly improve the light focusing intensity of the lens in a broad band of frequencies. This wonderful bioinspired phenomenon is expected to design more interesting and serviceable devices by combining photonic crystals with transformation optics.

Keywords: cats' eyes; Luneburg lens; tapetum lucidum; photonic crystals.

DOI: 10.3788/COL202220.012202

1. Introduction

Nature provides us a wealth of choices from micron to nanostructures, for templates of manufacturing a wide range of photonic structures[1–8]. For example, the butterfly[9–11], beetle[12], and tapetum lucidum of many vertebrates' eyes[13,14] are typical examples. Like other vertebrates' eyes, tapetum lucidum of cats' eyes is made of photonic crystals, which is a reflective layer behind the retina. As a mirror reflecting light back to the retina, it offers a second chance for the photoreceptor cells to stimulate again, thereby enhancing the sensitivity of the retina. Due to this reflection structure, light will be reflected from cats' eyes, causing a conspicuously bright spot which looks sparkling[15–17]. Observed with an electron microscope, tapetum lucidum cells as a kind of photonic crystals are characterized by periodically arranged parallel rod-shaped inclusions[18], which exhibit photonic bandgaps and could be used to manipulate the flow of light[19–22]. Some previous works utilized this structure to design the retroreflector, which can redirect the incident wave back toward the source in the direction antiparallel to the incident direction. Conventional retroreflectors can work within limited incident angles[23,24], which can be overcome by taking advantage of a Luneburg lens[25]. All of these works have something in common, whose reflective layer is simply substituted for a metallic mirror, high reflective coating, or metasurfaces rather than photonic crystals. Here, we try to devise the retroreflector by combining the Luneburg lens and photonic crystals and investigate the characteristics behind them.

In optics, on the other hand, absolute optical instruments are widely used in many fields with characteristics of perfect imaging or self-imaging[26–30]. For example, the Luneburg lens as an absolute optical instrument plays an important role in geometric optics. It is a spherical dielectric with a refractive index profile, which can focus a parallel beam of light into a point without abbreviation[31]. We thereby utilize this special property of the Luneburg lens to simulate retinal imaging for bionic research.

In this Letter, we analyze the structure and photonic bandgaps of tapetum lucidum. Enlightened by the specialty of tapetum lucidum, we leverage the Luneburg lens and photonic crystals to mimic the process of the effect of retroreflector and light focusing and explore the intensity enhancement in visible light. Besides, we do some improvements to increase the stability of the effect. From these, we reveal in some measure why tapetum lucidum is so efficient to reflect light and improve light focusing intensity and have a deeper understanding of cats' eyes from the optics perspective.

2. Results

Firstly, let us consider the structure of a cat's eye in detail. The left part of Fig. 1 demonstrates the structure of a cat's eye, and the right one shows the schematic details of tapetum lucidum. As a reflective layer, tapetum lucidum is situated external to the retina, which can reflect light back onto the photoreceptors in the retina. Histologically, the cat's tapetum lucidum consists of 10–12 layers of cells in its center, and each cell consists of 15–20 layers of rods, progressively thinning and eventually disappearing towards the periphery[15–17]. For the perfect presentation of figures, we draw three layers, and others are omitted in the right of Fig. 1. Tapetum lucidum is filled with many dense

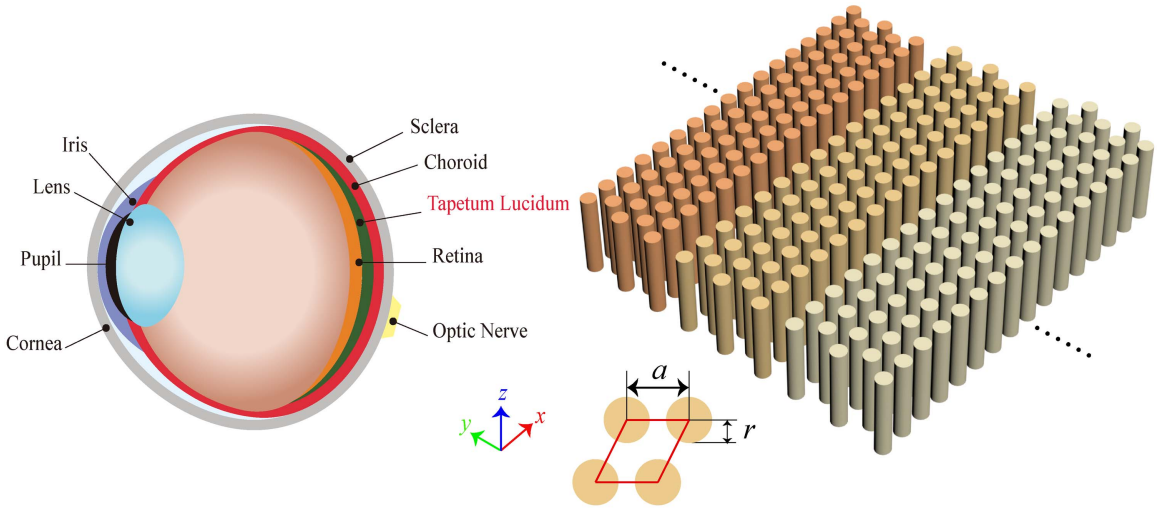

Fig. 1. Structures of a cat's eye (left picture) and tapetum lucidum (right picture). The tapetum lucidum lies behind the retina constituted by some columnar photonic crystals arranged in regular hexagons with different radii r and spaces a.

small rods with a length of 4–6 μm and a radius r of 0.05–0.06 μm, which are precisely arranged in a hexagonal lattice pattern with the space of a between adjacent rods of about 0.15 μm. These rods are grouped in bundles, normally extending through the entire thickness of the cell, whose main components are riboflavin and zinc (the refractive index of the compound is approximately 1.8). Within each bundle, the center of the rods is aligned parallel to the surface of the retina with obvious regularity[15–17].

If we want to investigate the light propagation in photonic crystals, what we have to do is to calculate the corresponding photonic band structures. Hence, in order to be closer to reality, we choose different spaces of rods of 0.15 μm, 0.20 μm, and 0.25 μm to calculate the band structure, with their radius as 0.05 μm. Except for rods, the refractive index of the remaining parts of tapetum lucidum is about one, so we put some triangular array medium columns (refractive index $n = 1.8$) in the air background when simulating.

Photonic crystals possess different complete photonic bandgaps, as described by different colors in Fig. 2. The bandgaps for the case of $a = 0.15$ μm is from 333 nm to 375 nm, for the case of $a = 0.20$ μm is from 375 nm to 441 nm, and for the case of $a = 0.25$ μm is from 441 nm to 517 nm, whose working wavelengths do not overlap with each other. When the wavelength falls in a photonic bandgap, light will be bounced back such that it provides a second opportunity to stimulate the photoreceptor cells, thereby enhancing the sensitivity of the retina and improving the night vision ability of cats[17]. Consequently, we can design an artificial "tapetum lucidum" with the data above in the following sections. There are some similarities and differences between the tapetum lucidum and artificial "tapetum lucidum." The arrangement (hexagon) and layer structure are the same, while the size of rods and number of layers are different. For tapetum lucidum, there are hundreds of layers of rods, the space (about $a = 0.15$ μm) and the size (about $r = 0.05$–0.06 μm) of each rod are not exactly the same, and thus, the structure is aperiodic. For the artificial "tapetum lucidum," we simply take an approximate space and size for consideration in order to facilitate the analysis of its band structure. Considering simulation limitations, we only arranged three layers of photonic crystals behind the Luneburg lens with the spaces of 0.15 μm, 0.20 μm, and 0.25 μm. In order to achieve the intensity enhancement in a broader band of frequencies, we simulate with the increasing space a. In fact, the space is not increased as the layers go away from the lens in the tapetum lucidum.

Now, we perform the simulations using the finite element software COMSOL Multiphysics. In simulations, we suppose the waves are in transverse electric (TE) polarization (the electric fields are along the z direction). In Fig. 3, we would like to mimic cats' eyes by using the Luneburg lens, mimic light incident

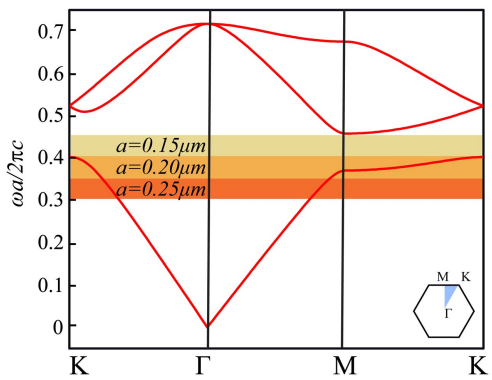

Fig. 2. Photonic band structures for transverse electric (TE) modes of a triangular array of medium columns (refractive index $n = 1.8$, $r = 0.05$ μm) in the air. The inset at the corner shows the high symmetry points of the irreducible Brillouin zone (shaded light blue one). Note that complete photonic bandgaps happen for different colors with $a = 0.15$ μm, $a = 0.20$ μm, and $a = 0.25$ μm.

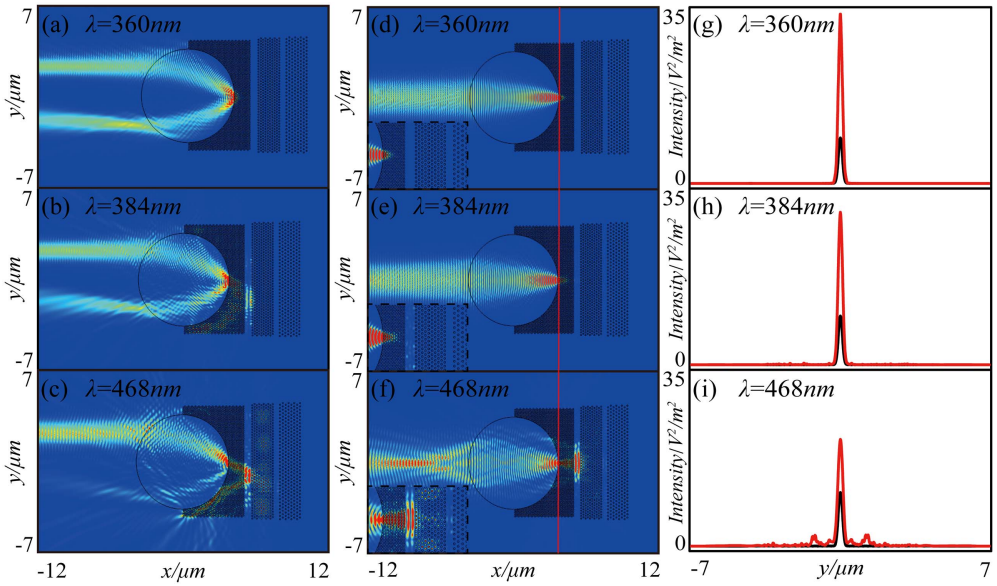

Fig. 3. Electric field intensity $|E|^2$ distributions of a Gaussian beam impinging on the Luneburg lens and the corresponding intensity comparison chart. (a)–(c) The electric field intensity of a Gaussian beam impinging on the Luneburg lens along $y = 2$ μm with different wavelengths. (d)–(f) The electric field intensity of a Gaussian beam impinging along the x axis, and the red line is along $x = 3.5$ μm. The detailed field distributions are inserted at the bottom of each figure, which are marked by the black dashed frames. (g)–(i) Intensity comparison with (red curves) and without (black curves) photonic crystals along the red line of (d)–(f).

to cats' eyes by using an impinged Gaussian beam along the x direction, and mimic tapetum lucidum by using photonic crystals. The radius and refractive index profile of the Luneburg lens were set as $r_0 = 3.5$ μm and $n(r_1) = \sqrt{2 - r_1^2/r_0^2}$, respectively. Afterwards, we placed different-space rods ($r = 0.05$ μm) with $a = 0.15$ μm (first layer), $a = 0.20$ μm (second layer), and $a = 0.25$ μm (third layer) from left to right behind the Luneburg lens to replace tapetum lucidum, just as the data provided in Fig. 2. In Figs. 3(a)–3(c), we impinged Gaussian beams with three different wavelengths towards the Luneburg lens. The wavelengths were in the above three photonic bandgaps, respectively. When the wavelength falls in the photonic bandgap of the first layer, waves will be completely blocked by the first layer, and the device seems like an Eaton lens [Fig. 3(a)][32]. Hence, the Luneburg lens plus a layer of photonic crystals can achieve the effect of an Eaton lens. If the wavelength falls in the photonic bandgap of the second and third layers [Figs. 3(b) and 3(c)], waves will transmit through the first layer and be reflected by the second or third layer. So, from the bionic research simulation, it is easy to understand why there are hundreds of layers of rods in cats' tapetum lucidum, which can reflect about 130 times of light more than that of human eyes and with a very broad band of working wavelengths[33].

Considering simulation limitations, we arranged three layers of photonic crystals behind the Luneburg lens. Although the number of layers we simulated is limited, it can still explain why there is a luminous look in cats' eyes at night in some degree. In addition, riboflavin as the main component can absorb light in short wavelengths such as blue light and emits fluorescence in the wavelengths of green light. That is why we often see cats' eyes appear turquoise.

If we impinge Gaussian beams with three different wavelengths along the x axis in Figs. 3(d)–3(f) towards the Luneburg lens, waves will be blocked by photonic crystals and focus at the point (3.5,0). Therefore, by comparing the intensity with and without photonic crystals along the red line $x = 3.5$ μm, we can plot a comparison chart in Figs. 3(g)–3(i), where the focusing curve becomes sharper, as we expected with the help of photonic crystals. In order to make a better analysis of the field distribution in the photonic crystals, the detailed field distributions are inserted at the bottom of Figs. 3(d)–3(f), which are marked by the black dashed frames. We see that the field is localized at the first layer when the wavelength is 360 nm, as shown in Fig. 3(d). If the wavelength falls in the photonic bandgap of the second or third layer [Figs. 3(e) and 3(f)], waves will transmit through the first layer and be reflected by the second or third layer. Therefore, field distributions exist between the layers in Figs. 3(e) and 3(f). Exactly as light blocked by tapetum lucidum can focus on the retina again, waves blocked by photonic crystals focus at the point (3.5,0) as well. Hence, the sensitivity of the retina and the electric field intensity of the point (3.5,0) are enhanced apparently. Compared to the Luneburg lens without photonic crystals [the black lines of Figs. 3(g)–3(i)], the focusing curves of the Luneburg lens with photonic crystals [the red lines of Figs. 3(g)–3(i)] become sharper. As shown in Figs. 3(g)–3(i), the peaks of black lines are always below the red lines. Therefore, it can explain clearly that the structure of photonic crystals behind the Luneburg lens can improve the intensity.

Our simulations, to some extent, illustrate why cats can distinguish things clearly even in a poor light environment. In other words, the intensity of the Luneburg lens without photonic crystals represents the intensity of the poor light environment.

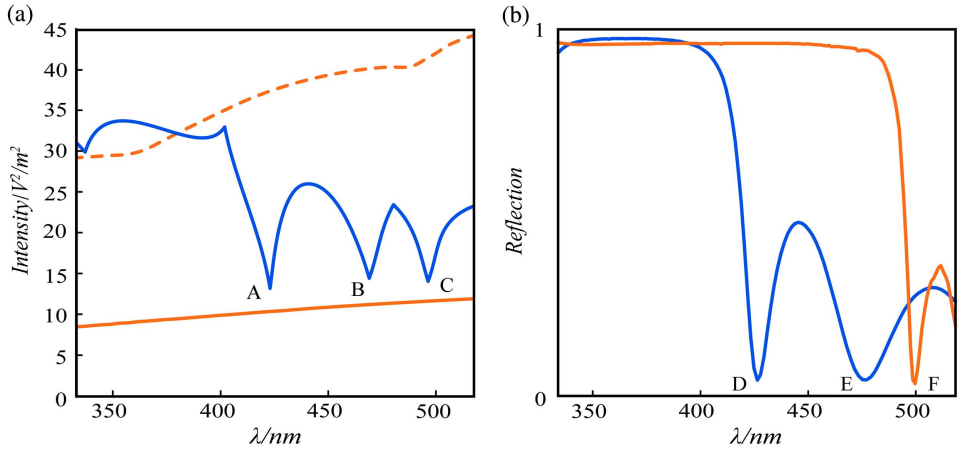

Fig. 4. Intensity comparison from 333 nm to 517 nm at the point (3.5, 0) and the reflectance of photonic crystals. (a) The solid blue and orange lines denote the intensity with and without photonic crystals, respectively. The dashed orange line denotes the intensity with PEC. (b) The solid blue and orange lines denote the reflectance of one layer and two layers of photonic crystals, respectively.

Even through the Luneburg lens (cats' eyes) in a poor light environment, the intensity can be improved with the photonic crystals (tapetum lucidum).

Based on the simulation results we obtained above, we attempt to realize this in other wavelengths and compare the electric field intensities. As shown in Figs. 3(g)–3(i), we obtain the intensity statistics of comparison with and without photonic crystals along $x = 3.5$ μm. In Fig. 4, we select the electric field intensity at the point (3.5,0) and plot them with respect to different wavelengths. As we predicted, for the wavelength from 333 nm to 400 nm, the electric field intensity can approximately reach about 30 V^2/m^2, which is three times more than that without photonic crystals. From 400 nm to 517 nm, the blue line fluctuates but is also above the solid orange line. We display the intensity of the Luneburg lens plus the perfect electric conductor (PEC) using the orange dashed line in Fig. 4(a) and perceive that both the Luneburg lens with photonic crystals (solid blue line) and PEC (orange dashed line) can achieve the intensity enhancement and account for the validity of our bioinspired design. Besides, we calculate the reflectance of one layer (first layer $a = 0.15$ μm) and two layers (first layer $a = 0.15$ μm and second layer $a = 0.20$ μm) and detect that the wavelengths of fluctuation points in Fig. 4(a) (A, B, and C) are coincident with the points (D, E, and F) in Fig. 4(b). For wavelengths less than that of point D (or A), it falls into the bandgap of the first layer. The dip at point B is caused by Fabry–Perot (FP) resonance of the first layer, which is denoted by point E. For wavelengths less than that of point F (or C), it falls into the bandgap of the second layer. Hence, we can understand that because of the low reflection of the corresponding wavelength and the resonance between layers, the curve displays notable oscillations. The first layer of photonic crystals plays a deciding role in intensity enhancement.

Therefore, the light focusing intensity of the lenses is greatly improved in a broad band of frequencies inspired by cats' eyes. This reaffirms our idea that cats allow for the detection of light that is imperceptible to the human eyes because of the hundreds of layers of photonic crystals in tapetum lucidum.

There is a possibility the solid orange line would be above the blue line when the wavelength is large enough. As we can see from the blue line in the Fig. 4(a), the farther the layer from the Luneburg lens is, the worse the effect will be. As the wavelength increases, the layer is farther and farther away from the Luneburg lens, so it has the potential to be absolute that the solid orange line would be above the blue line. In this Letter, we only consider the case of three layers, and the solid orange line is always below the blue line.

Except for TE polarization, we also attempted the transverse magnetic (TM) polarization (the magnetic fields are along the z direction) and found that for both TE and TM waves the structures can achieve the intensity enhancement. For simplicity, we show the TE polarization as an example in this Letter.

Only the wave both impinging and blocked by photonic crystals focusing at the point (3.5,0) can get the purpose of intensity enhancement. For the structure of Fig. 3, if we change the incident angles, the focusing intensity will decrease. Hence, we do some improvements based on the structure in Fig. 3, and the intensity can be increased even if the incident angle is changed. As shown in Figs. 5(d)–5(f), the retroreflector is composed of two elements: a Luneburg lens and three arcual structures with the same radii and spaces as in Fig. 3. Along the red line, we can plot comparison chart in Figs. 5(g)–5(i), where the focusing curve becomes sharper, and the intensity is enhanced for the different incident angles (the incident angle is defined as the deviation angle from the geometric symmetric axis of the structure, with the up deviation angle as "+"). From the simulation results, we can observe obviously that the improvement is effective and increases the stability of the effect compared to the structure in Fig. 3. Here, we choose 25 deg as an example in Fig. 5. If we use the plane wave as the source, the results of intensity enhancement also can be achieved, as shown by Figs. 5(a)–5(c).

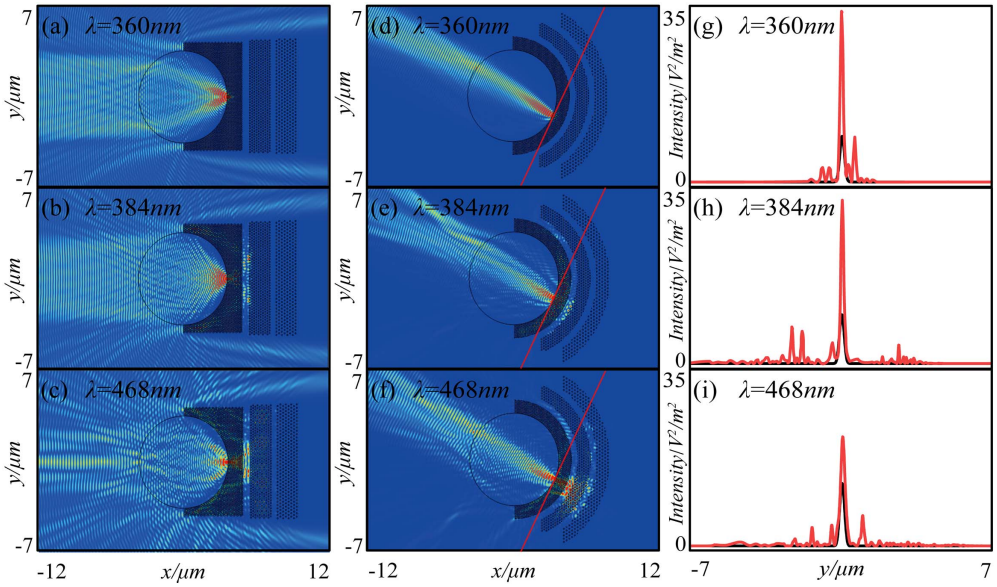

Fig. 5. Electric field intensity $|E|^2$ distributions of a plane wave and a Gaussian beam impinging on the Luneburg lens and the corresponding intensity comparison chart. (a)–(c) The electric field intensities of the plane wave impinging on the Luneburg lens. (d)–(f) The electric field intensities of a Gaussian beam impinging on the Luneburg lens at 25° with different wavelengths. (g)–(i) Intensity comparison with (red curves) and without (black curves) photonic crystals along the red lines of (d)–(f).

3. Conclusion

Our bionic research not only allows people to better understand why cats can accurately capture prey even in a poor light environment and cats' eyes often flash at night from the perspective of photonic crystals, but also confirm that the first layer of photonic crystals of cats' eyes plays a deciding role in intensity enhancement. Based on the structure of tapetum lucidum, we integrate similar photonic structures to the Luneburg lens, and the focusing intensity is greatly improved in a broad band of frequencies. Furthermore, the effect of the retroreflector can also be demonstrated via this design. Thus, the integration of photonic crystals into the Luneburg lens shows the practicability and availability, which is a magical collision of photonic crystals and transformation optics. The amazing animal world has taught us a lot, and there are many more interesting optics phenomena that deserve to be explored in future.

Acknowledgement

This work was supported by the National Key Research and Development Program of China (No. 2020YFA0710100), the National Science Foundation of China (Nos. 11874311 and 92050102), and the Fundamental Research Funds for the Central Universities (No. 20720200074).

Reference

1. S. A. Davis, S. L. Burkett, N. H. Mendelson, and S. Mann, "Bacterial templating of ordered macrostructures in silica and silica-surfactant mesophases," Nature **385**, 420 (1997).
2. G. Cook, P. L. Timms, and C. Göltner-Spickermann, "Exact replication of biological structures by chemical vapor deposition of silica," Angew. Chem. Int. Edn. **42**, 557 (2003).
3. R. Seshadri and F. C. Meldrum, "Bioskeletons as templates for ordered, macroporous structures," Adv. Mater. **12**, 1149 (2000).
4. S. Chia, J. Urano, F. Tamanoi, B. Dunn, and J. I. Zink, "Patterned hexagonal arrays of living cells in sol–gel silica films," J. Am. Chem. Soc. **122**, 6488 (2000).
5. D. Yang, L. Qi, and J. Ma, "Eggshell membrane templating of hierarchically ordered macroporous networks composed of TiO_2 tubes," Adv. Mater. **14**, 1543 (2002).
6. A. Dong, Y. Wang, Y. Tang, N. Ren, Y. H. Zhang, Y. H. Yue, and Z. Gao, "Zeolitic tissue through wood cell templating," Adv. Mater. **14**, 926 (2002).
7. A. R. Parker, "Natural photonics for industrial inspiration," Philos. Trans. Royal Soc. A: Math. Phys. Eng. Sci. **367**, 1759 (2009).
8. S. Tadepalli, J. M. Slocik, M. K. Gupta, R. R. Naik, and S. Singamaneni, "Bio-optics and bio-inspired optical materials," Chem. Rev. **117**, 12705 (2017).
9. P. Vukusic, J. R. Sambles, and C. R. Lawrence, "Colour mixing in wing scales of a butterfly," Nature **404**, 457 (2000).
10. L. P. Biró, Z. Bálint, K. Kertész, Z. Vértesy, G. I. Márk, Z. E. Horváth, J. Balázs, D. Méhn, I. Kiricsi, V. Lousse, and J.-P. Vigneron, "Role of photonic-crystal-type structures in the thermal regulation of a Lycaenid butterfly sister species pair," Phys. Rev. E **67**, 021907 (2003).
11. J. Huang, X. Wang, and Z. L. Wang, "Controlled replication of butterfly wings for achieving tunable photonic properties," Nano Lett. **6**, 2325 (2006).
12. A. R. Parker, V. L. Welch, D. Driver, and N. Martini, "Opal analogue discovered in a weevil," Nature **426**, 786 (2003).
13. M. F. Land and D.-E. Nilsson, *Animal Eyes* (Oxford University, 2012).
14. M. F. Land, "The physics and biology of animal reflectors," Prog. Biophys. Mol. Boil. **24**, 75 (1972).
15. M. H. Bernstein and D. C. Pease, "Electron microscopy of the tapetum lucidum of the cat," J. Biophys. Biochem. Cytol. **5**, 35 (1959).
16. J. A. Coles, "Some reflective properties of the tapetum lucidum of the cat's eye," J. Physiol. **212**, 393 (1971).
17. F. J. Ollivier, D. A. Samuelson, D. E. Brooks, P. A. Lewis, M. E. Kallberg, and A. M. Komáromy, "Comparative morphology of the tapetum lucidum (among selected species)," Vet. Ophthalmol. **7**, 11 (2004).
18. F. G. Omenetto, "Photonics in nature—opportunities and challenges at the biological interface," APL Photon. **4**, 070402 (2019).

19. S. John, "Strong localization of photons in certain disordered dielectric superlattices," Phys. Rev. Lett. **58**, 2486 (1987).
20. E. Yablonovitch, "Inhibited spontaneous emission in solid-state physics and electronics," Phys. Rev. Lett. **58**, 2059 (1987).
21. R. D. Meade, J. N. Winn, and J. D. Joannopoulos, *Photonic Crystals: Molding the Flow of Light* (Princeton University, 1995).
22. J. Sheng, J. Xie, and J. Liu, "Multiple super-resolution imaging in the second band of gradient lattice spacing photonic crystal flat lens," Chin. Opt. Lett. **18**, 120501 (2020).
23. A. Arbabi, E. Arbabi, Y. Horie, S. M. Kamali, and A. Faraon, "Planar metasurface retroreflector," Nat. Photon. **11**, 415 (2017).
24. T. Takatsuji, M. Goto, S. Osawa, R. Yin, and T. Kurosawa, "Whole-viewing-angle cat's-eye retroreflector as a target of laser trackers," Meas. Sci. Technol. **10**, N87 (1999).
25. Y. Fu, J. Li, Y. Xie, C. Shen, Y. Xu, H. Chen, and S. A. Cummer, "Compact acoustic retroreflector based on a mirrored Luneburg lens," Phys. Rev. Mater. **2**, 105202 (2018).
26. U. Leonhardt and T. Philbin, *Geometry and Light: The Science of Invisibility* (Courier Corporation, 2010).
27. T. Tyc, L. Herzanova, M. Sarbort, and K. Bering, "Absolute instruments and perfect imaging in geometrical optics," New J. Phys. **13**, 115004 (2011).
28. L. Xu and H. Chen, "Conformal transformation optics," Nat. Photon. **9**, 15 (2015).
29. J. B. Pendry, "Negative refraction makes a perfect lens," Phys. Rev. Lett. **85**, 3966 (2000).
30. H. Chen and W. Xiao, "Morse lens," Chin. Opt. Lett. **18**, 062403 (2020).
31. R. K. Luneburg, *Mathematical Theory of Optics* (University of California, 1966).
32. J. Eaton, "On spherically symmetric lenses," Trans. IRE Prof. Group Antennas Propag. **PGAP-4**, 66 (1952).
33. R. W. Rodieck, "The vertebrate retina: principles of structure and function," Arch. Ophthalmol. **58**, 948 (1974).